ROYAL SOCIETY
OF CHEMISTRY

PAPER

Check for updates

Enhancing gamma-irradiated NBR/PVC blends with sulfur nanoparticles as a crosslinking promoter

Doaa S. Mahmoud,[a] Mohamad Bekhit, [ID] *[b] Salwa H. El-Sabbagh[a] and E. S. Fathy [ID] [c]

The development of polymer nanocomposites is crucial for meeting increasing industrial demands. This research investigated the use of synthesized sulfur nano-particles (S-NPs) as a vulcanizing agent in acrylonitrile butadiene rubber (NBR) and polyvinyl chloride (PVC) blends, which were subsequently exposed to 50 kGy of gamma irradiation. Structural analyses (XRD, TEM, and SEM/EDX) confirmed the formation and dispersion of S-NPs. The influence of S-NP content and gamma irradiation (50 kGy) on the mechanical performance, crosslinking characteristics, and thermal-aging resistance of the blends was systematically investigated. Compared with the pristine NBR/PVC blend, the incorporation of S-NPs significantly enhanced tensile strength from 2.75 MPa to 6.56 MPa and 6.38 MPa for blends containing 0.5 and 2 phr of S-NPs, respectively, under irradiation. After thermal aging at 100 °C, the tensile strength reached up to 9.10 MPa for S-NP-based vulcanizates. Equilibrium swelling decreased from 270% to 120% before irradiation and from 255% to 105% after irradiation, consistent with increased crosslink density and improved mechanical performance. Furthermore, gamma irradiation synergistically enhanced the material properties, as evidenced by the reduced swelling percentage with the increasing S-NP content, indicating higher crosslink density. The blends also exhibited strong resistance to thermal aging at 100 °C and to brake oil, making S-NP-vulcanized NBR/PVC blends suitable for applications in the production of model car tires and footwear, combining the flame resistance of PVC with the flexibility of NBR.

1. Introduction

Gamma irradiation modification of rubber and plastic composites has attracted increasing attention due to their significant changes in their properties without affecting the polymer composition and with no harmful byproducts. When polymers are exposed to radiation, the crosslinking is induced which enhance the comptability between the various components of the composite and consequently improves their overall mechanical, chemical, and thermal properties. The gamma irradiation technique confers environmental benefits by minimizing toxic emissions, thereby offering a precise and cleaner alternative to conventional chemical crosslinking methods. Moreover, gamma radiation is one of the most popular electromagnetic radiations for the sterilization of polymeric materials such as disposable medical equipment.[1–6]

Polymer blending is an essential approach to creating new materials whose properties are designed to differ from those of the separate components. This approach is a cost-effective method compared with the costly synthesis of completely new

polymers. Due to their versatile and beneficial characteristics, polymer blends are accepted in many industrial arenas. Their advantages in these applications have been established with improved optical, electrical, structural, thermal, and mechanical properties.[7,8]

Nitrile rubber, or acrylonitrile–butadiene rubber (NBR), is created through the reaction of the monomers butadiene and acrylonitrile. This rubber has excellent anticorrosion properties and is highly resistant to oil. These characteristics are the main reasons for the extensive use of NBR in the automobile and aerospace industries. Nevertheless, due to the presence of unsaturation in its structure, NBR exhibits poor aging resistance, which limits its applications. To increase the properties and service life of NBR, blending with other polymers is applied. NBR is often blended with various polymers, notably poly(vinyl chloride) (PVC), which improve its resistance to ozone and thermal aging as well as its mechanical properties.[9,10] PVC is a widely utilized thermoplastic owing to its low cost, processability, and versatility in both rigid and flexible forms. Its applications include construction, medical, electronic, and aerospace industries because of its flame retardancy and resistance to chemicals and environmental stress. PVC/NBR blends are known as a thermoplastic elastomer in which NBR acts as a permanent plasticizer for PVC in applications such as wire and cable insulation, food containers, and pond liners. Simultaneously, the PVC plastic phase improves the ozone and

[a]*Polymers and Pigments Department, National Research Centre, Giza, Egypt*

[b]*Radiation Chemistry Department, National Center for Radiation Research and Technology, Egyptian Atomic Energy Authority, Cairo, Egypt. E-mail: mohammed_bakhit2006@yahoo.com*

[c]*Polymer Chemistry Departments, National Center for Radiation Research and Technology, Egyptian Atomic Energy Authority, Cairo, Egypt*

chemical resistance as well as the thermal aging of NBR in applications such as gaskets, fuel hose covers, conveyor belt covers, and printing roll covers.[11–13] Additionally, PVC/NBR blends are particularly noteworthy for their excellent radiation durability and predominant crosslinking upon irradiation.[14–16]

One crucial step in the creation of rubber goods is vulcanization. One of the most popular vulcanizing agents in the rubber sector is sulfur. Sulfur creates a crosslinked network structure and crosslink the rubber molecular chain during vulcanization. Conventional sulfur vulcanization in elastomeric systems is often limited by poor sulfur dispersion and reduced crosslinking efficiency, particularly in heterogeneous polymer blends, such as NBR/PVC. Reducing sulfur to the nanoscale offers a potential route to overcome these limitations by increasing surface area and promoting a more uniform distribution within the polymer matrix. Sulfur nano-particles (S-NPs) are therefore expected to enhance crosslinking efficiency at lower loadings and improve interfacial interactions between blend components. This provides the rationale for investigating S-NPs as an advanced vulcanizing agent in NBR/PVC blends, especially in combination with radiation-induced crosslinking to further control network formation.[17,18] Recently, nano-sulfur decorated graphene oxide materials were employed by Qin et al. as a crosslinker for natural rubber (NR). The results showed that the NR containing nano-sulfur decorated graphene oxide was superior, exhibiting 31.1% and 12.8% higher tensile strength and tearing property, respectively, than NR containing an untreated graphene oxide.[19]

Despite extensive studies on the radiation-induced crosslinking of NBR/PVC blends, the potential role of sulfur nanoparticles as a vulcanizing agent under gamma irradiation remains largely unexplored. Most existing reports focus on conventional sulfur systems or irradiation effects in isolation, without addressing the combined influence of sulfur at the nanoscale and radiation on blend performance and stability. In this study, sulfur nano-particles (S-NPs) were introduced as a novel vulcanizing agent in NBR/PVC blends and evaluated under a moderate gamma irradiation dose (50 kGy). Owing to their high specific surface area, S-NPs are expected to promote a more efficient crosslinking at reduced loadings, while their interaction with gamma irradiation enables the formation of a more effective crosslinked network. This combined approach provides new insights into the enhancement of the mechanical strength, thermal stability, and solvent resistance of irradiated NBR/PVC blends in a more efficient manner.

2.   Experimental studies

2.1.   Materials

Sodium thiosulfate pentahydrate [(Na$_3$S$_2$O$_3$·5H$_2$O), purified and crystallized; molecular weight: 248.18 g mol^{-1}] was procured from PROLABO, France. Hydrochloric acid (35.4%) was obtained from S D Fine-Chem Limited (India). Bidistilled water was utilized throughout the preparation steps. Nitrile butadiene rubber (NBR34/45) with an acrylonitrile content of 34% ± 1% was supplied by Bayer AG Germany. It has a density of 0.99 g cm^{-3}. Poly(vinyl chloride) (PVC, k68) was supplied by

an Egyptian company for plastic industries and has a K-value of 68. Analytical grades of stearic acid (SA), zinc oxide (ZnO), and conventional accelerated sulfur (CS) were purchased from Sigma-Aldrich. TMQ (polymerized 2,2,4-trimethyl-1,2-dihydroquinoline) and CBS (N-cyclohexyl-2-benzothiazole sulfenamide) were utilized as antioxidants and accelerators, respectively. Dioctyl phthalate (DOP, technical grade), serving as the plasticizer, was supplied by Misr El-Hegaz Group, Egypt. Ba/Cd/Zn carboxylate was used as a heat stabilizer for PVC. Silica (Hi-Sil 233D), a white powder, was supplied by PPG Industries Inc., Netherlands (Europe). The coupling agent 3-(trimethoxy-silyl)-propylamine was supplied by Merck. All chemicals were used as received, without further purification. The DOT 4 brake oil was commercially supplied by Misr Petroleum (Egypt) and used as received without further purification.

2.2.   Methods

2.2.1.   Synthesis of sulfur nano-particles (S-NPs). Sulfur nanoparticles were prepared via acidification of sodium thiosulfate solutions.[19–21] First, 12.4 g of sodium thiosulfate (0.025 M) was dissolved in 1800 ml bidistilled water under magnetic stirring at room temperature for 30 min. Then, 200 ml (0.5 M) of HCl was added to this solution under continuous stirring. The ratio of the molar concentration of sodium thiosulfate to HCl was 1 : 2. The solution color changed from colorless to turbid yellow, confirming the successful formation of sulfur nanoparticles. The sulfur nanoparticles were separated via decantation and filtration, washed several times with bidistilled water till pH neutrality was obtained, and finally dried at room temperature for 24 h. The obtained yield of the sulfur nanoparticles was nearly 10% of the total dissolved sodium thiosulfate.

2.2.2.   Preparation of gamma-irradiated thermoplastic vulcanizates based on NBR/PVC blends. NBR and PVC were melt-mixed at a fixed blend ratio using an internal mixer (Brabender Plasticorder, C.W., Brabender Instruments Inc., South Hackensack, NJ, USA) with a mixing chamber capacity of 80 cm^3. The blending process was conducted at a temperature of 190 °C and a rotor speed of 30 rpm to ensure a homogeneous dispersion. The mastication of NBR was performed for 2 minutes, and silica, a coupling agent, and TMQ were subsequently added to the masticated rubber. Mixing was performed for 5 min, after which the pre-masticated NBR was combined with the PVC, and then the mixing process proceeded for additional 3 min. A heat stabilizer was subsequently introduced into the mixing chamber, after which mixing was carried on for an additional minute. Finally, accelerators were incorporated, followed by CS and the prepared S-NPs, and the mixing was continued until the compound was homogenous. After that, the blending products were put on a plate vulcanizing press and vulcanized for t_{c90} min at 152 °C. To investigate the impact of ionizing radiation, the fabricated NBR/PVC blend compounds were subjected to 50 kGy of gamma irradiation from a Co-60 source (Gamma Cell 220, MDS Nordion, Canada) at the Egyptian Atomic Energy Authority.[15] The samples were irradiated at

Table 1 Composition of NBR/PVC blend vulcanizates

Blend constituents/phr	NV_0	$NVcS_{0.5}$	$NVnS_{0.5}$	$NVnS_1$	$NVnS_{1.5}$	$NVnS_2$
NBR	70	70	70	70	70	70
PVC	30	30	30	30	30	30
ZnO	5	5	5	5	5	5
Stearic acid (SA)	2.5	2.5	2.5	2.5	2.5	2.5
Coupling agent	3	3	3	3	3	3
Silica	40	40	40	40	40	40
DOP	11	11	11	11	11	11
Heat stabilizer	1	1	1	1	1	1
TMQ	0.8	0.8	0.8	0.8	0.8	0.8
CBS	0.6	0.6	0.6	0.6	0.6	0.6
Commercial sulfur (C-S)	—	0.5	—	—	—	—
Sulfur nano-particles (S-NPs)	—	—	0.5	1	1.5	2

room temperature with a calibrated dose rate of 0.604 kGy h^{-1}. The required dose was obtained by adjusting the time of exposure, according to the dose rate, to deliver the required absorbed dose. All the steps are illustrated in Table 1 and Scheme 1.

2.3. Characterization techniques

An X-ray diffractometer (XRD, Shimadzu 6000, Japan), fitted with a Cu Kα (1.5418 Å) X-ray source, was used to analyze the X-ray diffraction of synthesized samples. High-resolution transmission electron microscopy (HRTEM) images using a JEOL
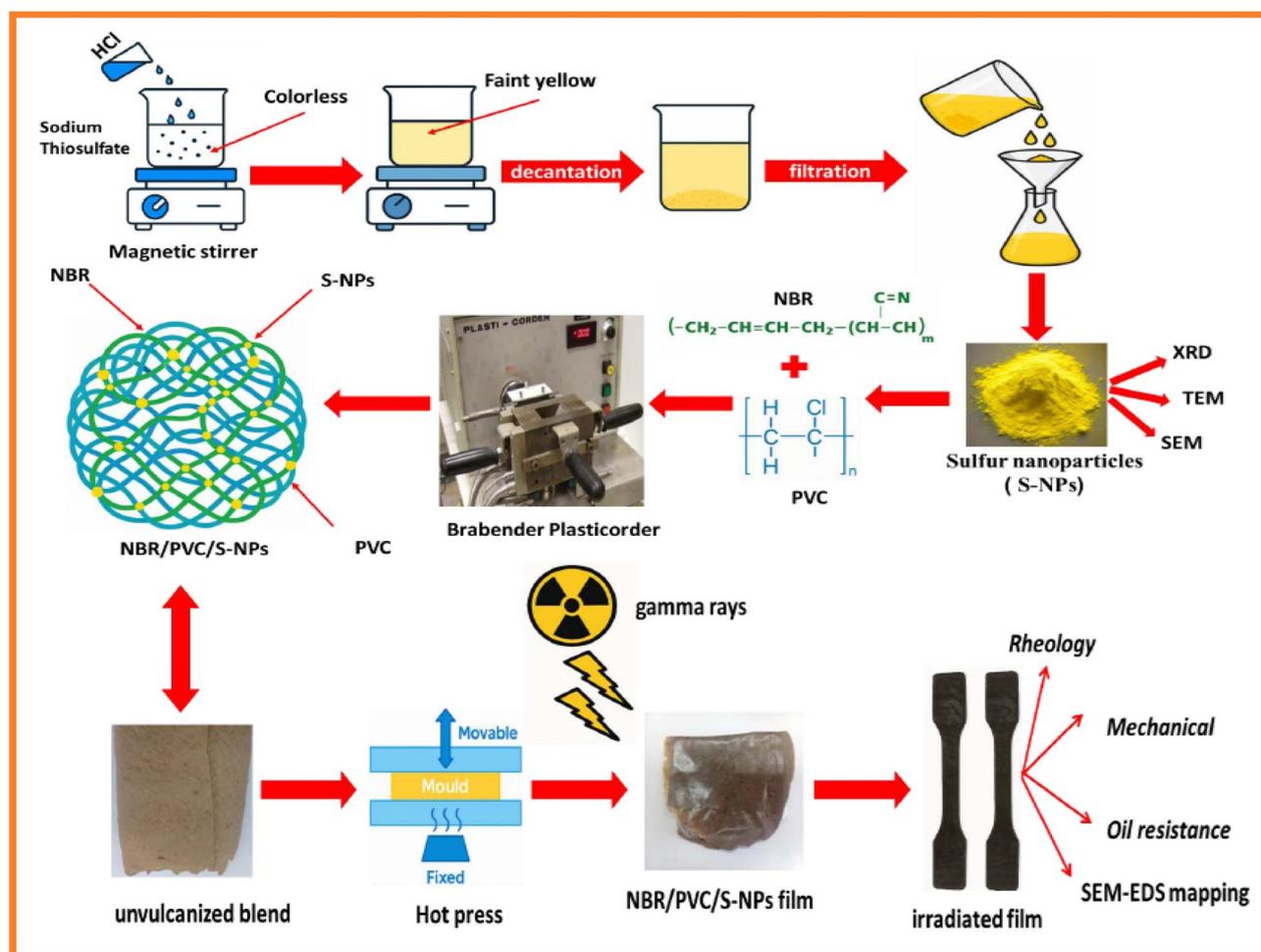
Scheme 1 Preparation steps of the sulfur nanoparticles and the gamma-irradiated NBR/PVC blend vulcanizates.

JEM-2100 F microscope (Japan) operating at an accelerating voltage of 200 kV were used to observe the size and shape of the synthesized nanoparticles. A scanning electron microscope (SEM) (ZEISS EVO-15V, UK) in conjunction with an energy-dispersive X-ray spectroscopy (EDX) probe was used to obtain both the surface morphology and EDX analysis of the synthesized nanoparticles. On the other hand, the distribution of S-NPs on the NBR/PVC blend surface was examined using a scanning electron microscope (SEM, Quanta FEG 250).[22] The Fourier transform infrared (FTIR) spectra of the NBR/PVC blends were obtained using an ATR PRO450-S instrument with a single-reflection ATR attachment. The curing characteristics of the compounds were determined using a Monsanto oscillating disc rheometer (model 100, Akron, USA). The NBR/PVC blend compounds were vulcanized using an electrically heated laboratory hydraulic press in accordance with ASTM D2084-11 (2011). The vulcanization process involved the application of 4 MPa pressure at a temperature of 152 °C ± 1 °C, with curing times ranging from 14 to 35 minutes, depending on the specific material and rheometric readings. The plaque dimensions for the process were 15 cm × 15 cm × 0.2 cm ($L \times B \times H$).[23] The mechanical properties of the blend compounds were evaluated using a Zwick testing equipment in accordance with ASTM D412-16. The tests were carried out at a speed of 500 mm min^{-1} under controlled ambient temperature conditions of 24 °C ± 2 °C. Five dumbbell-shaped specimens were prepared per formulation to ensure testing consistency.[23,24]

The swelling behavior and crosslink density of the NBR/PVC blend vulcanizates were evaluated in accordance with ASTM D471 by immersing pre-weighted samples in 100 ml of toluene until the swelling percentage was obtained. The specimens were removed, blotted to eliminate surface solvent, weighed, and dried, and the swelling percentage was computed using the following equation:

$$\text{Swelling percentage} = \frac{W_S - W_d}{W_d} \times 100 \tag{1}$$

where W_S denotes the swollen weight after immersion time t and W_d represents the dried weight. Using the equilibrium swelling data, the crosslink density was subsequently evaluated using the following Flory–Rehner equation:[25]

$$M_c = -\frac{\rho_R V_1 \left(V_r^{1/3} - \dfrac{V_r}{2} \right)}{\ln(1 - V_r) + V_r + \mu V_r^2} \tag{2}$$

where V_1 is the molecular volume of toluene ($V_1 = 106.35$ cm^3 mol^{-1}), ρ_R is the density of the rubbers, M_c is the molecular weight between crosslinking density (g mol^{-1}), and μ denotes the Flory–Huggins interaction parameter. The crosslink density was calculated using the Flory–Rehner equation in accordance with ASTM D6814 based on equilibrium swelling measurements obtained using ASTM D471.[24]

$$\nu = \left(\frac{1}{2M_c} \right) \tag{3}$$

To determine the interactions between NBR/PVC blends and sulfur nanoparticles (S NPs), thermodynamic parameters including the Gibbs free energy (ΔG) and the entropy (ΔS) were estimated using the Flory–Huggins's equation (eqn (4)):

$$\Delta G = RT\{\ln(1 - V_r) + V_r + \mu V_r^2\}. \tag{4}$$

Here, T denotes the absolute temperature ($T = 25$ °C + 273.15 = 298.15 K); R, the universal gas constant (8.314 J mol^{-1} K^{-1}); and V_r, the volume fraction of the blend compounds in the swelling phase.[22] The conformational entropy (ΔS) that represent the number of accessible spatial configurations of the polymer chain can be calculated using the following equation (eqn (5)).[23]

$$\Delta S = -\Delta G/T \tag{5}$$

The total insoluble content of the NBR/PVC blends was obtained *via* solvent extraction in accordance with ASTM D2765. Samples were taken after sulfur curing and irradiation, cut into small pieces, and dried to a constant weight (W_0). Subsequently, the specimens were removed, blotted to eliminate the surface solvent after 24 h, and then oven-dried at 50–60 °C until a constant mass (W_d) was achieved.

The total insoluble content (gel fraction) was calculated using the following equation:

$$\text{The total insoluble content} = W_d/W_0 \times 100 \tag{6}$$

The soluble fraction (%) was calculated according to the following equation:

$$\text{Soluble fraction (\%)} = 100 - \text{total insoluble content (\%)} \tag{7}$$

All measurements were performed three times, and the average of the three independent results was calculated and reported.

The NBR/PVC blends containing S-NPs were aged according to ASTM D573-99 (Standard Test Method for Rubber Deterioration in an Air Oven) for hot air aging, where the blends were exposed to hot air at 100 °C for 24 hours. Mechanical properties were assessed after aging. Additionally, both irradiated and non-irradiated blends were also aged in a vacuum oven at 100 °C for 24 hours to simulate different conditions. The oil resistance of the NBR/PVC blend compounds was evaluated by soaking each sample separately in a brake oil for 4 weeks at room temperature. Using a digital balance, the weight in air (m_0) of the unirradiated and irradiated samples was first determined. Following immersion, the samples were taken out, gently wiped with filter paper to eliminate extra oil, and weighed once more (m_t). After that, the proportion of swelling was determined as follows:

$$S\% = \frac{m_t - m_0}{m_0} \times 100 \tag{8}$$

3. Results and discussion

3.1. Powder X-ray diffraction (PXRD)

The XRD analysis of the sulfur nanoparticles is illustrated in Fig. 1. As shown, the synthesized sulfur nanoparticles exhibit good crystallinity, and the peaks at $2\theta = 15.35°$, $21.84°$, $23.02°$, $24.86°$, $25.77°$, $26.68°$, $27.66°$, $28.63°$, $31.29°$, $34.06°$, $35.78°$, $36.98°$, $37.88°$, $39.25°$, $42.62°$, $45.52°$, $47.70°$, $51.10°$, $51.95°$, $52.95°$, $53.78°$ and $56.51°$ are attributed to the crystal planes of sulfur at 113, 220, 222, 133, 026, 311, 206, 313, 044, 137, 244, 317, 335, 02 10, 062, 408, 515, 357, 535, 602, 175 and 371, respectively. The diffraction peak positions and intensities agree well with the values reported in the literature for the orthorhombic structure of sulfur (JCPDS card no. 00-085-0799).[26–28] The sharp diffraction peaks indicating that sulfur nanoparticles have high crystallinity. The average crystallite size of the SNPs can be calculated using the Debye Scherrer formula, $D = K\lambda/\beta \cos\theta$, where K is the Scherrer constant or the shape factor $(=0.9)$, $\lambda = 1.5418$ Å is the X-ray wavelength, β is the full width at half maximum, θ is Bragg's diffraction angle, and D is the average crystal size.[29,30] Using the diffraction peak associated with the crystal plane (222), the crystallite size was estimated to be 45.75 nm for sulfur nanoparticles. The broadening of sulfur diffraction peaks indicating the lower particle size which reflect higher dispersion in polymer blends. The XRD analysis of sulfur nanoparticles measured after one year did not reveal any significant shift compared with the freshly prepared sulfur nanoparticles, indicating their high stability. Moreover, the diffraction peaks of the sulfur nanoparticles were more intense than those of commercial sulfur, indicating higher crystallinity. The formation mechanism of sulfur nanoparticles can be clarified according to the following equations (eqn (9) and (10)) where sodium thiosulfate in acidic media is converted into sulfur and sulfurous acid.[20,21]

$$Na_2S_2O_3 + 2HCl \rightarrow 2NaCl + SO_2 + S\downarrow + H_2O \quad (9)$$

$$SO_2 + H_2O \rightarrow H_2SO_3 \quad (10)$$
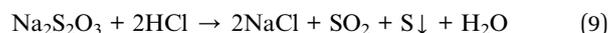
3.2. Analysis via electron microscopy (SEM and TEM)

The SEM images of the sulfur particles are presented in Fig. 2a–c. It is evident that the sulfur particles have a nearly uniform size and spherical shape. Also, the images show the presence of anisotropic sulfur particles produced during the nucleation and growth of sulfur particles.[31] The EDX technique was employed to determine the elemental constituent and purity of the tested sample. As shown in Fig. 2d, the EDX spectrum confirms the high purity of sulfur nanoparticles. Furthermore, it can be seen that commercial sulfur has multiple agglomerated particles with a diameter larger than that of sulfur nanoparticles. Swiderska-Mocek et al. found that the diameter of the precipitated sulfur was nearly one order of magnitude lower than that of commercial sulfur due to a relatively short time of sulfur crystal growth.[32]

Fig. 3a and b presents the particle size and shape morphology of S-NPs, as observed via TEM. The TEM images
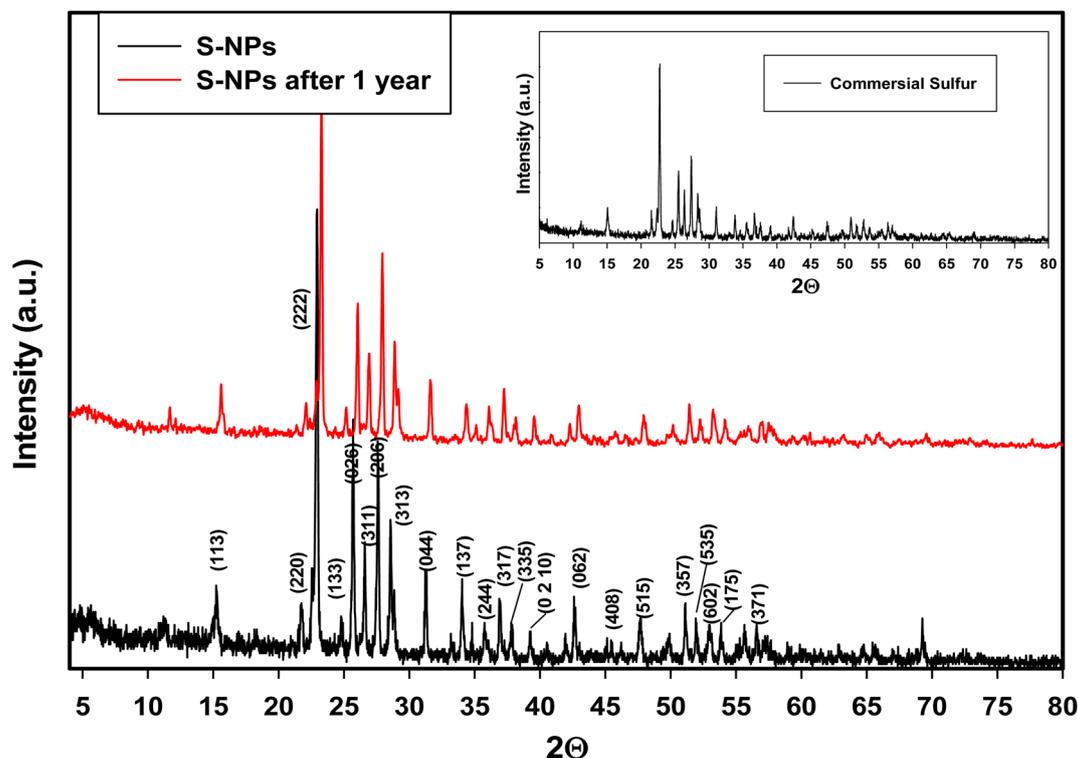

Fig. 1 XRD spectrum of the S–NPs and commercial sulfur (inset).
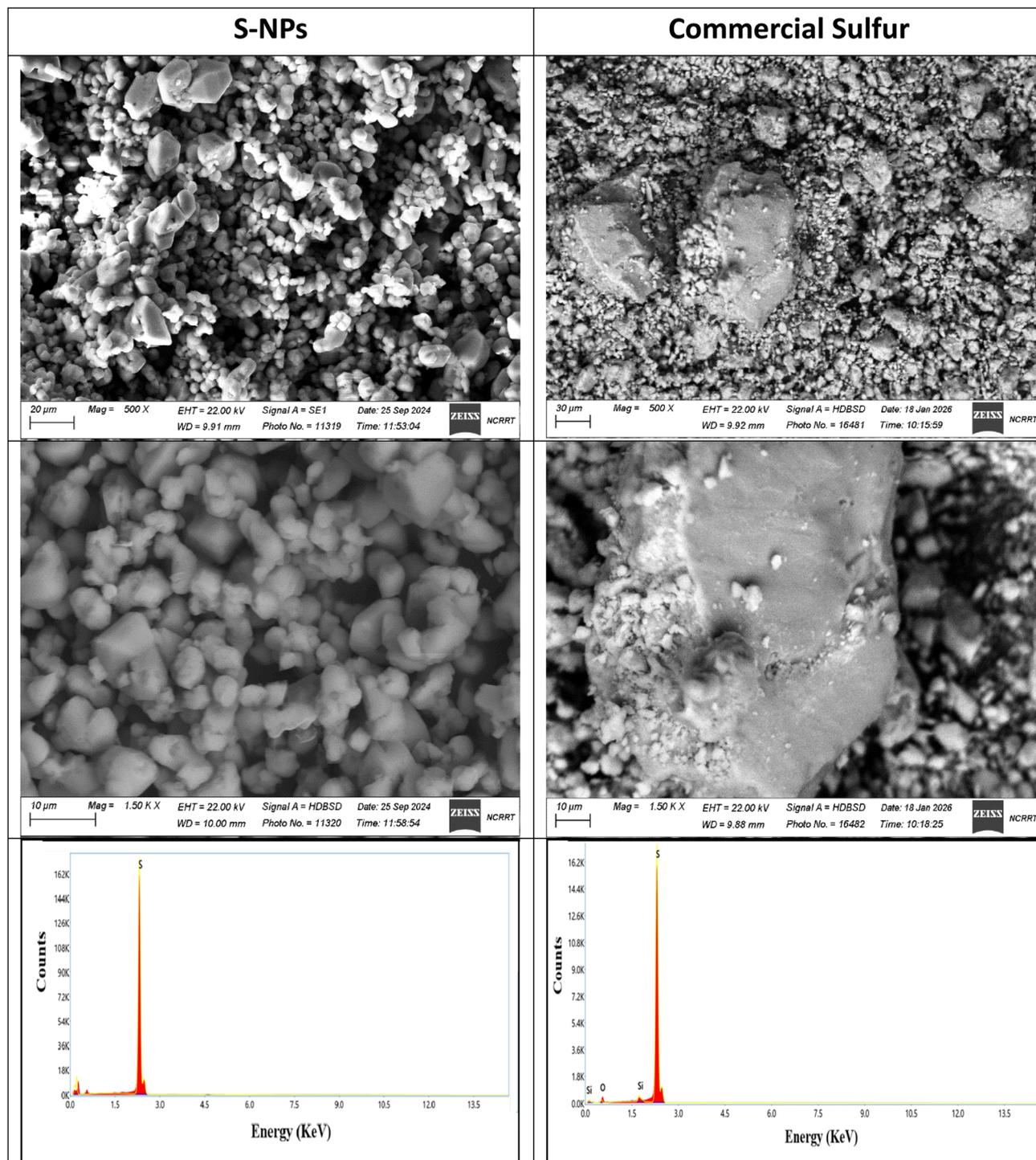
Fig. 2 SEM images with different magnifications and EDX images of commercial sulfur (right column) and SNPs (left column).

show that the S-NPs have a spherical shape and are conspicuously aggregated with an average diameter of *ca.* 90 ± 5 nm. Based on the SEM and TEM data, we can conclude that sulfur tends to aggregate. The aggregation is due to their high surface energy and the absence of a stabilizing agent.[33] On the other hand, the TEM images of commercial sulfur show a polydisperse nature and an agglomerated structure in a major micro scale and some spherical particles attached in an aggregated nanoscale (Fig. 3c and d).

3.3. Rheological properties

The quality of rubber products for home use is determined by the physical characteristics of rubber/plastic composites. Fig. 4 shows the rheometric curves of NBR/PVC composites filled with
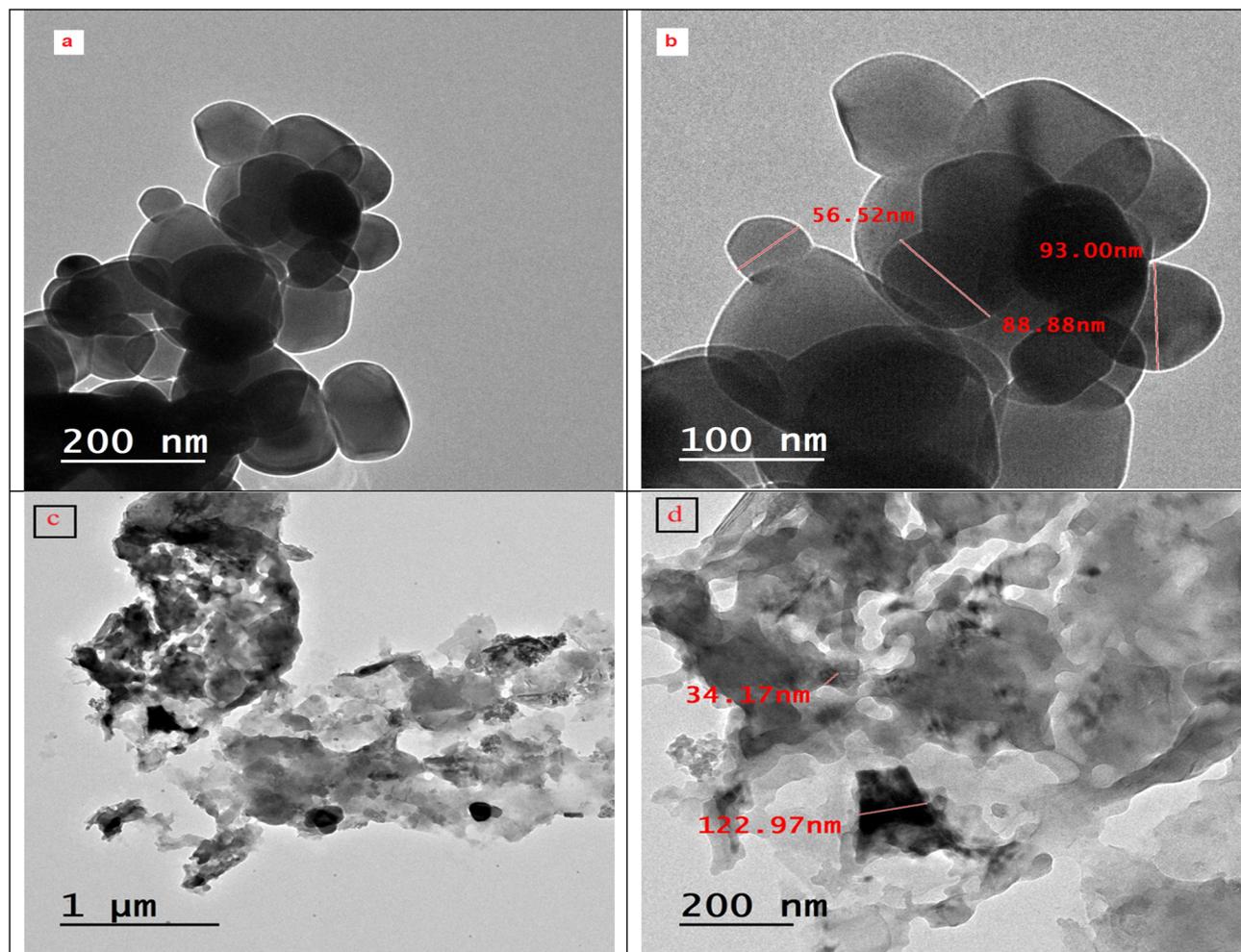
Fig. 3 TEM images with different magnifications of S–NPs (a and b) and commercial sulfur (c and d).

silica/silane coupling agent, incorporating different contents of S-NPs, 0.5 phr of commercial sulfur (C-S), or without sulfur. As shown in Table 2, incorporating 0.5 phr of S-NPs into the NBR/PVC composite increases the maximum torque (S'_{max}), minimum torque (S''_{min}), and torque difference while increasing the scorching time (t_{S2}) and cure rate index (CRI). At the same time, S-NPs reduce the optimum curing time (t_{c90}) and tan δ. Overall, the sample NVnS$_{0.5}$ exhibits greater rheological performance than NVcS$_{0.5}$ (commercial sulfur) or NV$_0$ (without sulfur). The higher scorching time in the NVnS is attributed to the interfacial physical interactions (mainly dipole–dipole interactions) between the polar nitrile groups of NBR and the C–Cl groups of PVC that slows down the initial vulcanization process.[34] Increasing the PVC content in NBR/PVC blends results in longer scorching and curing times due to the restricted mobility of NBR chains imposed by the PVC phase. This behavior confirms that PVC does not participate in sulfur crosslinking but rather influences the vulcanization kinetics of the NBR phase (Scheme 2).[34] This delayed curing promotes better compound formation and minimizes energy processing. Notably, NVnS$_{0.5}$ also exhibits a higher torque difference than NVcS$_{0.5}$ and NV$_0$, confirming better curing efficiency. The

crosslink density (torque difference) of NBR/PVC composites also affects the hardness value. The higher the crosslinking density, the lower the chain mobility.[35,36] The increased torque and reduced curing time in the composite containing 0.5 phr of S-NPs confirm that the vulcanization reaction is significantly enhanced compared to the composites containing commercial sulfur (C-S) or without sulfur (see Table 2). This indicates that S-NPs create stronger interfacial interactions than C-S particles because of their larger surface area, leading to a more effective vulcanization. According to Li *et al.*,[37] the incorporation of S-NPs increases the torque difference by enhancing the crosslink density. Their higher content provides additional sites during vulcanization, producing a denser and interconnected multi-phase network in the composites. At 0.5 phr, the S-NPs shortened the curing time (t_{c90}), whereas at higher contents (>1 phr) the curing time increased. The limited change at 1–2 phr reflects the competing effects of polarity and interactions with the polar NBR/PVC phases.[37] However, the S-NPs/NBR/PVC blend with silane-modified silica shows a decrease in t_{c90} at 0.5 phr, followed by an increase in t_{c90} as the S-NP loading rises. The longer t_{c90} in the S-NP/NBR/PVC blend is attributed to the neutralization of acidic S-NP surface groups and silanol with the
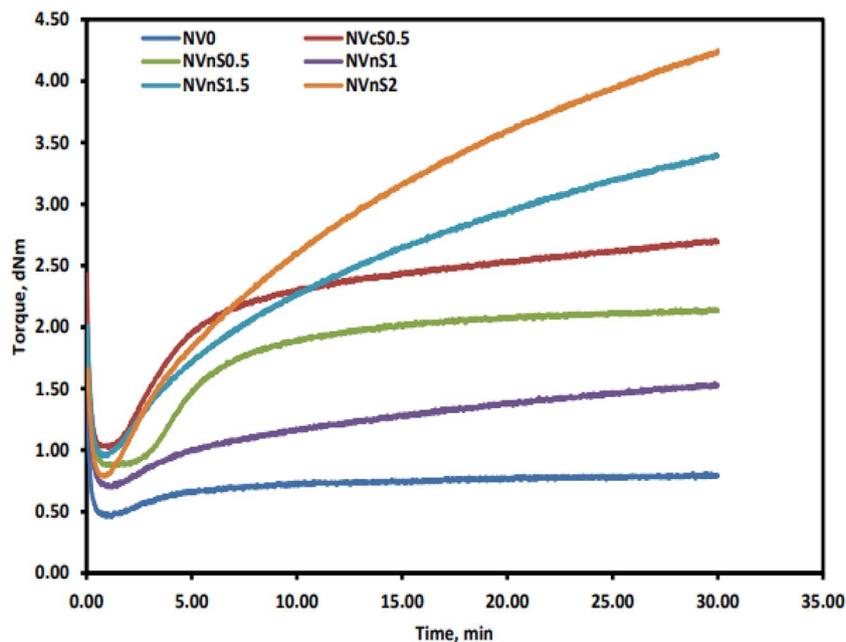
Fig. 4 Rheometric cure curves of the NBR/PVC blends obtained at a constant curing temperature, illustrating the evolution of torque with time and reflecting the curing behavior and crosslink development of the blends.

Table 2 Cure parameters for NBR/PVC composites at 152 °C

Blend constituents/properties	NV_0	$NVcS_{0.5}$	$NVnS_{0.5}$	$NVnS_1$	$NVnS_{1.5}$	$NVnS_2$
S'_{max} (dNm)	0.62	0.81	2.14	2.54	3.4	4.24
S''_{min} (dNm)	0.29	0.35	0.87	0.97	0.95	0.79
Torque difference (dNm)	0.33	0.46	1.27	1.54	2.45	3.45
t_{c90} (min)	34	18.17	14.79	24.09	24.13	24.21
t_{S2} (min)	0.98	3.83	4.765	9.53	10.02	11.43
CRI (min^{-1})	3.02	6.97	9.975	6.87	7.09	7.82
tan δ	3.105	1.837	1.7	1.854	1.946	1.942

activator and accelerator, which reduces the available sulfurating agents.[37] A shorter t_{c90} reflects a more efficient process and a better economy. The maximum torques of the NBR/PVC composite filled with modified silicate increased with the addition of the S-NPs. This effect could be due to the breakdown of agglomerates by the silane coupling agent.[37,38]
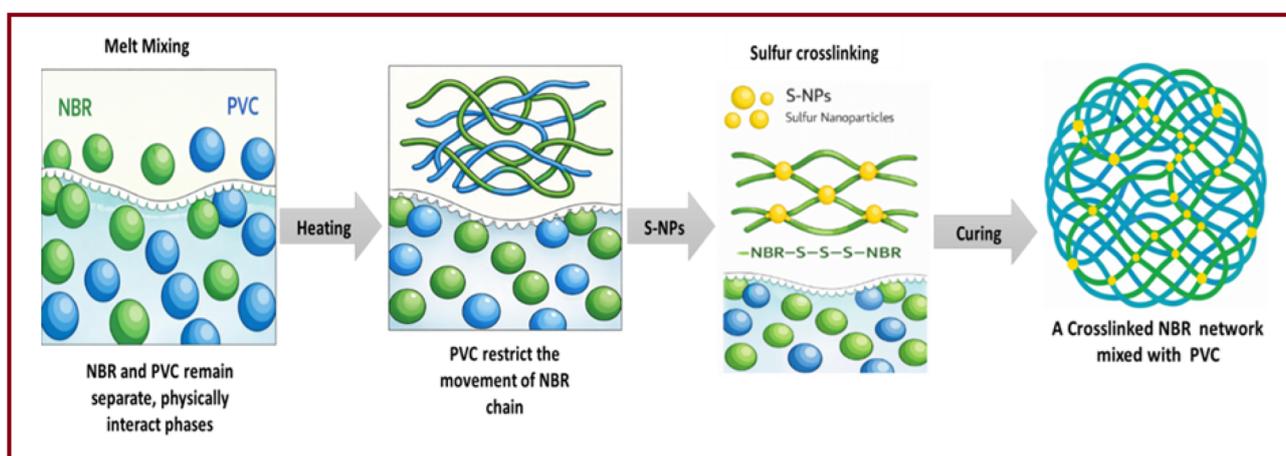
Scheme 2 Illustration of the curing process in the NBR/PVC blend.

tan δ is the ratio of the lost energy to the stored energy. It indicates energy dissipation, where higher values reflect greater molecular friction, resulting in greater energy dissipation and lower elasticity. Table 2 shows that increasing S-NPs generally raises tan δ in NBR/PVC composites because chain mobility becomes more restricted.

However, tan δ (damping coefficient) at a minimum torque is lower for $NVnS_{0.5}$ than for the other composites. tan δ is closely related to the degree of crosslinking, where a reduced damping factor suggests an enhanced crosslinking structure. On the other hand, higher torque difference (crosslink density) in $NVnS_{0.5}$ restricts chain mobility, increasing hardness and reducing tan δ (indicating lower energy dissipation).[35,36,39,40]

3.4. Mechanical properties

The mechanical properties of the fabricated blends depend on several factors, including the amount of filler distribution in the matrix–filler interface.[41–44] Table 3 displays the variation of tensile strength (TS), elongation at break, and modulus at different NBR/PVC blend elongations loaded with C-S and S-NPs. Mechanical investigations were carried out under a gamma irradiation dose of 50 kGy. The tensile strength of the pristine blend (2.6 MPa) remained nearly unchanged upon incorporation of 0.5 phr C-S (2.63 MPa), indicating limited reinforcement due to the poor dispersion and larger aggregate size of C-S. In contrast, the incorporation of S-NPs resulted in a pronounced and progressive enhancement in TS, reaching 4.42, 4.87, 7.88, and 9.1 MPa with increasing S-NP content. This significant improvement is attributed to the nanoscale size and homogeneous dispersion of S-NPs, which promote strong interfacial interactions and efficient stress transfer across the matrix–filler interface.[44] Furthermore, the S-NPs on the surface of the silane coupling agent are more homogenous and smaller than the C-S aggregates, improving the contact chance and creating advanced, uniform and efficient crosslinking active sites during the vulcanization process.[19] Furthermore, gamma irradiation contributes to additional crosslink formation within the NBR/PVC matrix, resulting in an enhanced tensile strength

for the irradiated blends, particularly at low C-S loading (0.5 phr) and S-NP content of up to 1 phr. The combined effect of radiation-induced crosslinking and S-NP-assisted interfacial reinforcement explains the observed mechanical performance enhancement, highlighting the superior reinforcing efficiency of S-NPs compared with C-S.

Table 3 also represents the elongation at break (%) values of the prepared blends before and after gamma irradiation. As observed, the elongation at break of the pristine NBR/PVC blend increases after gamma irradiation, which can be attributed to the crosslinking induced by radiation and partial chain alignment causing the hindrance of the mobility of the molecular chains. On the other hand, the incorporation of C-S and S-NPs leads to a reduction in the elongation at break. This behaviour is associated with increased crosslink density and enhanced matrix stiffness arising from improved filler dispersion and interfacial interactions, which restrict polymer chain mobility and reduce elastic deformation. The elastic modulus measured at different elongations follows a trend similar to that of tensile strength. The modulus increases with the addition of both C-S and S-NPs, reflecting the stiffening effect introduced to the polymer matrix through crosslinking and filler reinforcement. Notably, the NBR/PVC/S-NP composites exhibit the highest modulus values, which is attributed to the homogeneous dispersion and nanoscale reinforcing efficiency of S-NPs, resulting in effective load bearing and limited chain deformation under applied stress. The higher crosslink density caused by the sulfur nanoparticles and gamma irradiation, which limits polymer chain mobility, is responsible for the reduction in elongation at break. As a result, samples with higher modulus and tensile strength show fewer elongations at break, consistent with a network structure that is more tightly crosslinked.

The alterations of TS, elongation at break, and modulus at different elongation% (100%, 200%, and 300%) for samples after thermal aging at 100 °C are illustrated in Table 4. To determine the magnitude of the changes in the studied mechanical properties after thermal aging, the data recorded in Table 3 (mechanical parameters measured at room

Table 3 Mechanical properties of unirradiated and irradiated NBR/PVC blend vulcanizates

Blend constituents	Dose (kGy)	Tensile strength (MPa)	Elongation at break (%)	Modulus at 100% elongation, MPa	200% elongation, MPa	300% elongation, MPa
NV_0	0	2.75 ± 0.5	500 ± 20	0.53 ± 0.07	0.77 ± 0.026	1.01 ± 0.025
	50	4.2 ± 0.3	460 ± 35	0.58 ± 0.062	0.8 ± 0.048	1.04 ± 0.023
$NVcS_{0.5}$	0	2.44 ± 0.3	495 ± 40	0.53 ± 0.012	0.79 ± 0.31	1.04 ± 0.41
	50	4.57 ± 0.47	465 ± 53	0.67 ± 0.042	1.11 ± 0.036	1.51 ± 0.05
$NVnS_{0.5}$	0	4.24 ± 0.2	510 ± 85	1.01 ± 0.023	1.46 ± 0.086	1.89 ± 0.12
	50	6.56 ± 0.7	515 ± 91	1.29 ± 0.02	1.53 ± 0.05	1.96 ± 0.06
$NVnS_1$	0	4.23 ± 0.2	495 ± 54	0.86 ± 0.014	1.36 ± 0.016	1.83 ± 0.018
	50	5.22 ± 0.13	475 ± 20	0.96 ± 0.03	1.52 ± 0.05	1.77 ± 0.07
$NVnS_{1.5}$	0	5.05 ± 0.6	475 ± 70	0.89 ± 0.04	1.38 ± 0.013	1.83 ± 0.023
	50	4.5 ± 0.9	465 ± 32	0.96 ± 0.2	1.54 ± 0.33	2.1 ± 0.05
$NVnS_2$	0	6.3 ± 0.8	460 ± 60	0.93 ± 0.068	1.44 ± 0.086	1.94 ± 0.014
	50	6.38 ± 0.21	460 ± 49	1.06 ± 0.01	1.71 ± 0.03	2.3 ± 0.034

Table 4 Mechanical properties of unirradiated and irradiated NBR/PVC blend vulcanizates after thermal aging at 100 °C

Blend constituents	Dose (kGy)	Tensile strength (MPa)	Elongation at break (%)	Modulus at 100% elongation, MPa	200% elongation, MPa	300% elongation, MPa
NV_0	0	2.6 ± 0.032	520 ± 40	0.64 ± 0.072	1.04 ± 0.12	1.29 ± 0.17
	50	5.83 ± 0.14	640 ± 47	0.74 ± 0.065	1.11 ± 0.33	1.4 ± 0.32
$NVcS_{0.5}$	0	2.63 ± 0.94	500 ± 40	0.84 ± 0.32	1.3 ± 0.015	1.59 ± 0.02
	50	6.15 ± 0.26	495 ± 37	1.3 ± 0.02	2.3 ± 0.01	3.18 ± 0.05
$NVnS_{0.5}$	0	4.42 ± 0.72	510 ± 35	1.05 ± 0.34	1.66 ± 0.12	2.05 ± 0.8
	50	8.2 ± 0.32	525 ± 45	0.99 ± 0.21	1.5 ± 0.41	2.22 ± 025
$NVnS_1$	0	4.87 ± 0.14	520 ± 55	1.22 ± 0.076	1.7 ± 0.17	2.25 ± 0.27
	50	6.7 ± 0.38	485 ± 35	0.96 ± 0.026	1.6 ± 0.07	2.14 ± 0.11
$NVnS_{1.5}$	0	7.88 ± 0.35	530 ± 80	1.24 ± 0.145	1.69 ± 0.072	2.23 ± 0.08
	50	6.47 ± 0.16	485 ± 52	1.05 ± 0.05	1.7 ± 0.091	2.4 ± 0.12
$NVnS_2$	0	9.1 ± 0.59	540 ± 60	1.2 ± 0.012	1.78 ± 0.016	2.34 ± 0.019
	50	7.9 ± 0.98	465 ± 56	1.1 ± 0.07	1.8 ± 0.12	2.4 ± 0.18

temperature) and the data in Table 4 (mechanical parameters measured after thermal aging at 100 °C) should be compared. Mechanical properties are likely to deteriorate because of thermal aging. Generally, the tensile strength of NBR/PVC blends is not affected by the operating temperature of 100 °C. This is considered a good result, which indicates the complete homogeneity between blended constituents and C-S and S-NPs, facilitating the maintenance of equivalent performance at the operating temperature. On the other hand, the TS of the NBR/PVC/(0.5 phr) S-NPs after undergoing thermal aging exhibited the lowest reduction.

This may be good because the aging temperatures will not change the composite characters of NBR/PVC/(0.5 phr) S-NPs. Furthermore, the ionizing radiation assisted all irradiated specimens retaining their properties better than the un-irradiated samples due to crosslinks formed through irradiation. The last result confirms that NBR/PVC composites have high thermal stability attributable to the strong interaction and interfacial bonding between macromolecular chains of NBR and PVC ingredients when undergoing thermal aging and irradiation.[19,45] On the other hand, both elongation at break% and modulus at different percentages of elongation after thermal aging are not affected evidently. Interestingly, the elasticity and stiffness of the NBR/PVC blend and their sulfur-containing composites exhibit no significant alterations after thermal aging.

3.5. Swelling properties and thermodynamic study

The swelling characteristics of NBR/PVC composites were assessed using toluene as the swelling medium. The degree of interaction between the matrix and both the commercial and lab-synthesized sulfur nano-particles (S-NPs) was determined by measuring the equilibrium swelling ratio. The results indicated that composites incorporating S-NPs exhibited a markedly reduced equilibrium swelling capacity compared with those containing free sulfur or commercial sulfur (refer to Fig. 5a). A progressive increase in S-NP content led to a consistent decline in swelling behavior, which is attributed to enhanced crosslink density that limits solvent penetration into the composite matrix. This type of behavior suggests good dispersion and high interfacial interaction between the S-NPs and the NBR/PVC matrix, which encourages the formation of stable physical crosslinks between polymer chains.

As a result of this behavior, the equilibrium swelling of S-NP/NBR/PVC composites was reduced. In general, the crosslink density of a compound is an important factor of its mechanical properties.[46] It was observed that the introduction of PVC into blend compositions decreased the equilibrium swelling rate, penetration rate, and average diffusion coefficient.[47] The increase in S-NP content significantly increases the crosslink density of the NBR/PVC composite structures (Fig. 5b), thereby creating a more elastic network. Furthermore, the crosslinked structure restricts polymer chain expansion during toluene immersion and reduces solvent diffusion into the intermolecular spaces in the NBR/PVC matrix, ultimately decreasing the total swelling percentage.[48–50]

The total insoluble content of the NBR/PVC blends was measured after sulfur curing and gamma irradiation (50 kGy), as summarized in Table 5. After sulfur curing, the insoluble content varied with the blend composition, indicating differences in crosslink density induced by the sulfur curing system. The reference blend (NV_0) exhibited an insoluble content of 84.94%, while the other blends showed values ranging from 61.94% to 77.90%. After irradiation, the total insoluble content increased for all formulations, thereby confirming radiation-induced crosslinking. NV_0 showed a moderate increase from 84.94% to 86.77%, whereas the blends containing C-S and S-NPs exhibited more pronounced increases, particularly $NVcS_{0.5}$ (61.94% to 67.38%) and $NVnS_{0.5}$ (74.56% to 77.34%). Blends with higher S-NP contents ($NVnS_1$ to $NVnS_2$) showed gradual increases, reaching up to 80.14% for $NVnS_2$. Overall, sulfur curing combined with irradiation increased the soluble contents of all blends, demonstrating the synergistic effect of radiation crosslinking. This behavior is consistent with the reduced swelling and increased crosslink density observed for the irradiated samples.
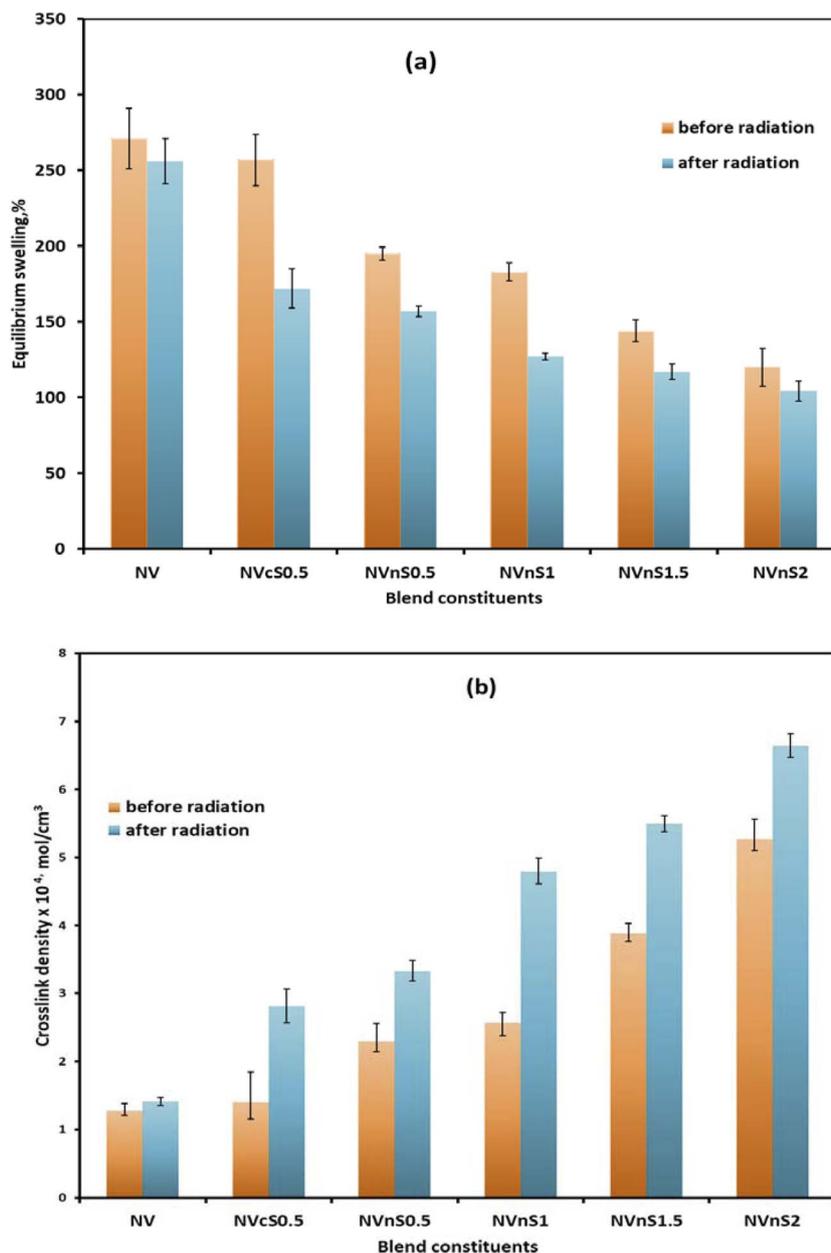
Fig. 5   (a) Equilibrium swelling percentage and (b) crosslink density of the unirradiated and irradiated NBR/PVC blend compounds, demonstrating the influence of irradiation on polymer network formation, solvent resistance, and crosslinking characteristics.

Table 5   Total insoluble content of NBR/PVC blends before and after irradiation

Blend constituents	Insoluble content (%) before radiation	Insoluble content (%) after radiation (50 kGy)
NV_0	84.94	86.77
$NVcS_{0.5}$	61.94	67.38
$NVnS_{0.5}$	74.56	77.34
$NVnS_1$	69.45	70.89
$NVnS_{1.5}$	73.77	74.2
$NVnS_2$	77.9	80.14

The thermodynamic effect was examined in order to ascertain how the NBR/PVC matrix and S-NPs interacted in the examined composite. The elastic Gibbs free energy (ΔG) and conformational entropy (ΔS) fluctuation of NBR/PVC composites are shown in Fig. 6. The statistical theory of rubber states that, the conformational entropy (ΔS) of various composites under investigation is related to the elastic Gibbs free energy (ΔG). The equation $-T = \Delta G/\Delta S$ predicts that the interior energy of the NBR/PVC network will not change as it extends.[39] The conformational entropy (ΔS) of NBR/PVC with 2 phr of S-NPs is clearly larger than that of NBR/PVC with silica filler without sulfur or commercial sulfur, as can be seen from Fig. 6. The main explanation for the higher value of ΔS in the NBR/PVC 2
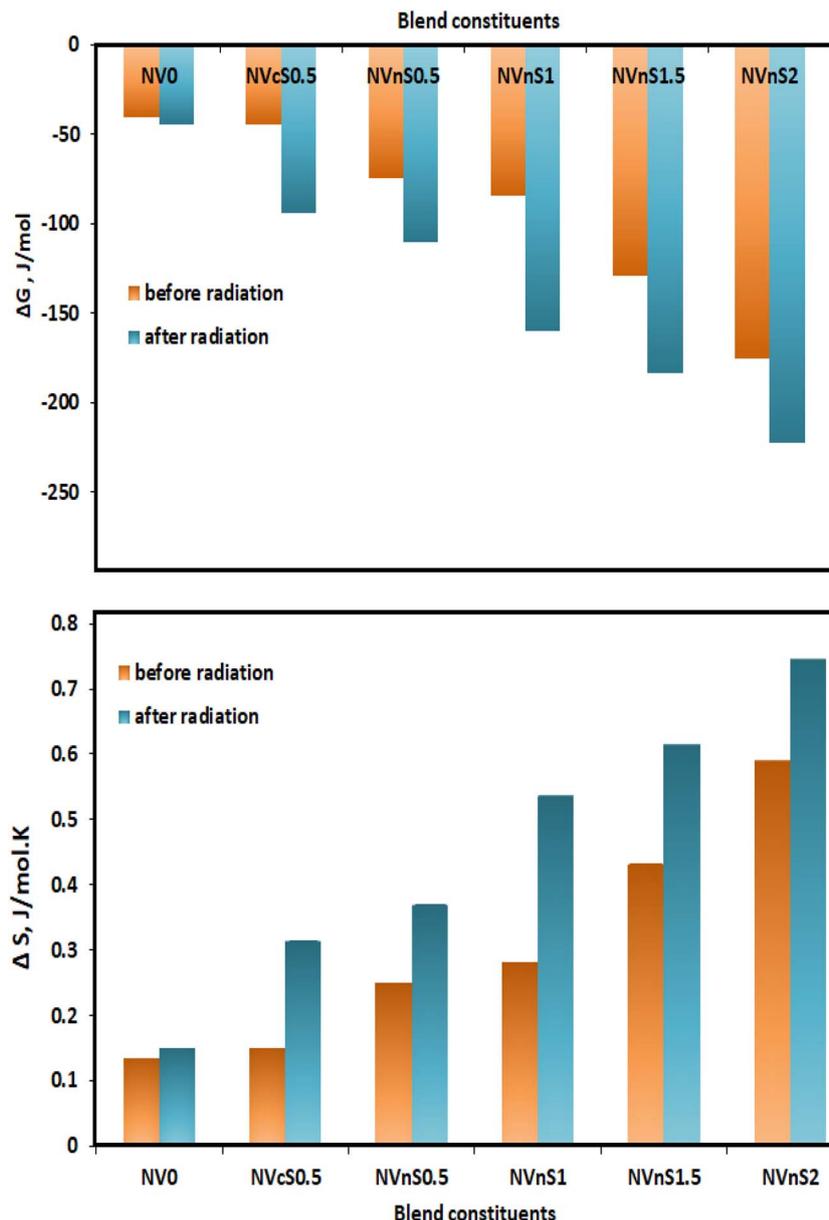
Fig. 6 The thermodynamic parameters, including Gibbs free energy change (ΔG) and entropy change (ΔS), of the unirradiated and irradiated NBR/PVC blend compounds, illustrating the influence of irradiation on the network structure and polymer–solvent interaction behavior.

phr of S-NPs is the homogeneous dispersion of S-NPs inside the NBR/PVC matrix. Again, for NBR/PVC composites, the value of ΔG is associated with the elastic properties of the composites.[22] Thus, the absolute value of ΔG visibly evidences the greater elastic behavior of NBR/PVC/2 phr S-NPs compared with NBR/PVC/other S-NP loading and NBR/PVC without sulfur or commercial sulfur. The improved elastic performance of the NBR/PVC composite containing 2 phr S-NPs is attributed to the enhanced compatibility between NBR/PVC matrix and S-NPs. Likewise, ΔG values become more negative as the concentration of NBR/PVC-based S-NPs increases. Increasing the S-NP content enlarges the interfacial area to some extent because of the reduced dispersed phase size caused by the filler.[22]

3.6. Oil resistance of fabricated blends

The oil resistance application of NBR/PVC blend nanocomposites based on swelling % in brake oil was studied. Fig. 7 explains the swelling percentage of NBR/PVC blend in the brake oil and the incorporation of C-S and S-NPs on the fabricated blends over 4 weeks. The incorporation of S-NPs led to a greater reduction in the swelling ratio of the NBR/PVC blend than that achieved with C-S. This could be due to the higher degree of dispersion of SNPs within the matrix compared with that of C-S. Moreover, it was shown that the interfacial bonding between the S-NP/silane coupling agent and the NBR/PVC matrix was stronger than that achieved in the conventional C-S vulcanization system. Furthermore, S-NPs are homogeneously anchored
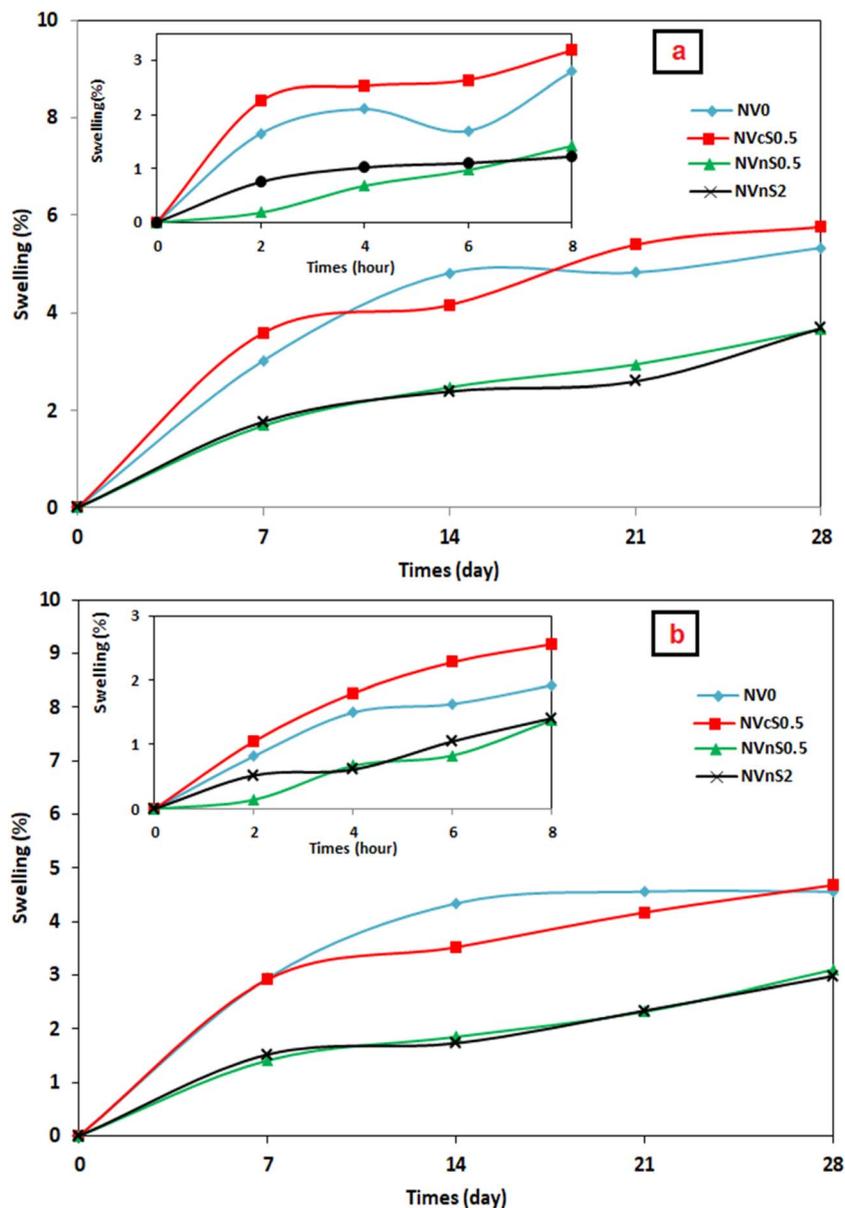
Fig. 7 Oil resistance (%) of the (a) unirradiated and (b) irradiated NBR/PVC blends after exposure to brake oil, illustrating the influence of irradiation on oil uptake and resistance performance.

onto the silane coupling agent, minimizing self-aggregation and enhancing their dispensability in the blend matrix. The last result coincides with that obtained by Qin *et al.*,[19] who reported that S-NPs are significantly smaller and more uniform in particle size than the conventional sulfur aggregates, enabling improved interfacial contact. Moreover, the swelling percentage of specimens studied in brake oil (pristine blend NBR/PVC, blend reinforced with commercial sulfur, and blend reinforced with nano-sulfur) reduced with the applied radiation dose. This behavior represents the formation of a denser crosslinked network within the matrix, which limits the diffusion of oil and improves oil resistance.[51]

3.7. FTIR analysis

The FTIR spectra of the NBR/PVC blend and its composites with sulphur (C-S and S-NPs), as well as before and after gamma irradiation, display the characteristic absorption peaks associated with the compatibility between NBR and PVC polymers. As shown in Fig. 8, all samples demonstrated distinct peaks at 2915 and 2845 cm^{-1}, which are related to aliphatic C–H stretch, whereas the bending vibrations of this group appear at 1100 cm^{-1}. The C–Cl stretching vibration appearing in the 600–700 cm^{-1} region confirms the presence of PVC. Furthermore, all the spectra demonstrated the disappearance of the distinct peak C≡N in NBR, which is located in the 2200–2260 cm^{-1} region in the FTIR spectra. This finding indicates the good computability and strong dipole–dipole interaction specifically
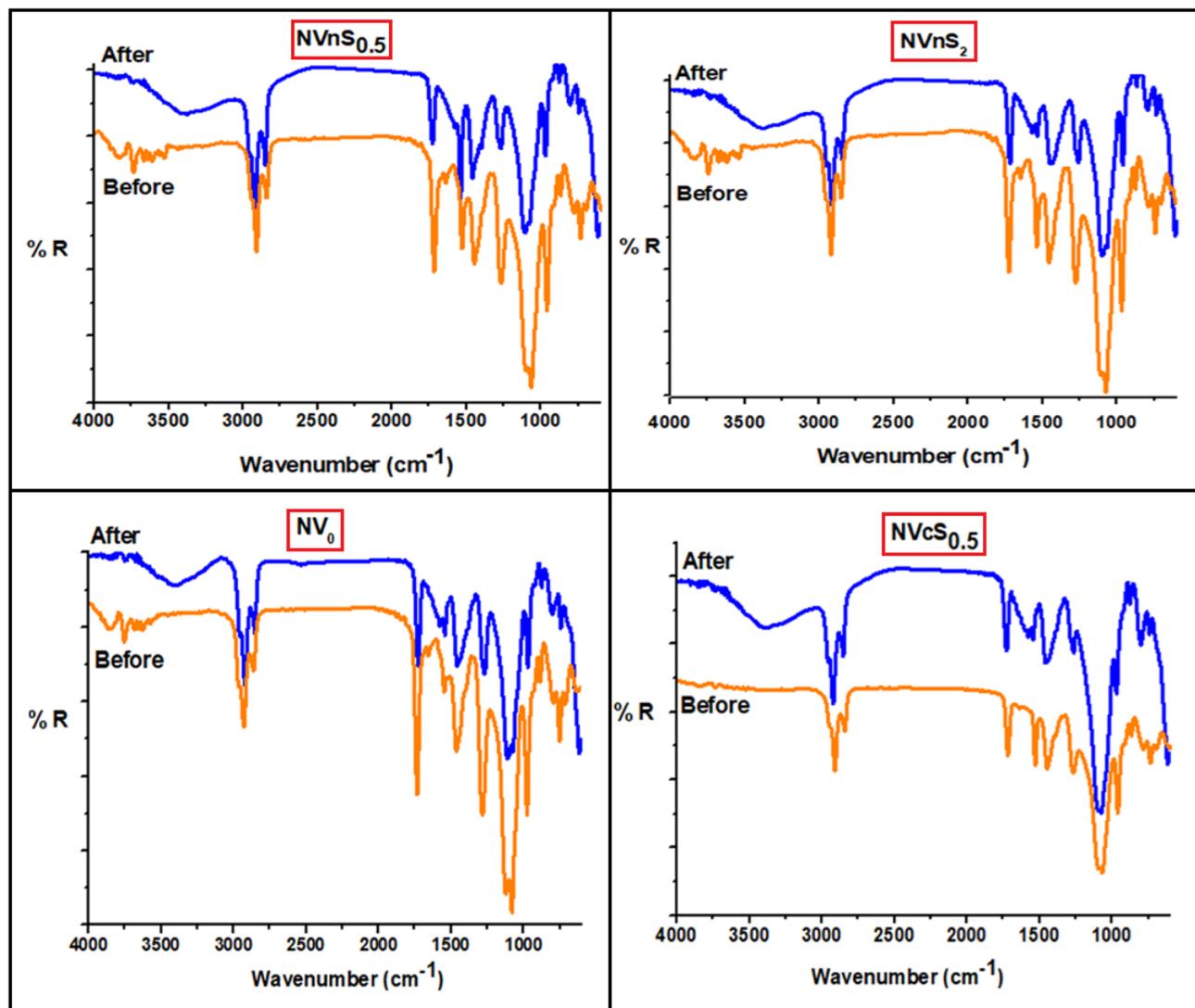
Fig. 8   FTIR spectra of the NBR/PVC blends before and after gamma irradiation in the absence and presence of vulcanizing agents (commercial sulfur and sulfur nanoparticles).

occurring between the polar nitrile groups of NBR and the C–Cl groups of PVC during the melt-mixing procedure. Thus, the C–N single bond strongly appears in all represented spectra at 1350 cm^{-1}. Therefore, during melt mixing, the weak triple- and double-bond CN are cleaved, whereas the strong single-backbone CN is maintained.[52]

Upon the addition of the vulcanizing agents (C-S and S-NPs), noticeable changes in band intensity and slight shifts in the C–H and C=C regions are observed, indicating the consumption of unsaturated sites and restricted chain mobility. Moreover, gamma radiation has produced a broad O–H absorption band in the range of 3500–3000 cm^{-1}; for all samples, it has also enhanced the C=C absorption band at 1635 cm^{-1}.[52] The changes in spectral appearance illustrated in Fig. 8 are the result of reactions that occur when radiation generates free radicals due to the scission of bonds (C–C and C–H) along the nitrile butadiene rubber (NBR) backbone. The free radicals that are generated eventually recombine and either form

intermolecular linkages or produce oxidized derivatives through interaction with oxygen, which ultimately results in the formation of a significant broadened –OH absorption band at 3500–3000 cm^{-1}.[53,54] Furthermore, after irradiation, the distinct absorption peak of C-S clearly appears at 700–750 cm^{-1} due to the role of sulfur in the formation of the network structure.

3.8.   Morphology of the blends

Elemental maps depicting the distribution of elements in the selected area are shown in Fig. 9, with a higher color intensity indicating a higher relative content. NV$_0$ (voids without sulfur), which mainly consists of carbon, oxygen, silica chlorine and zinc in accordance with the elemental composition of the NBR/PVC blend, is significantly observed. In the NVcS$_{0.5}$ region, the sulfur amount detected was less when compared with the NVnS$_{0.5}$ and NVnS$_2$ regions, which show differences in their compositions. Fig. 9 presents the SEM morphology of the
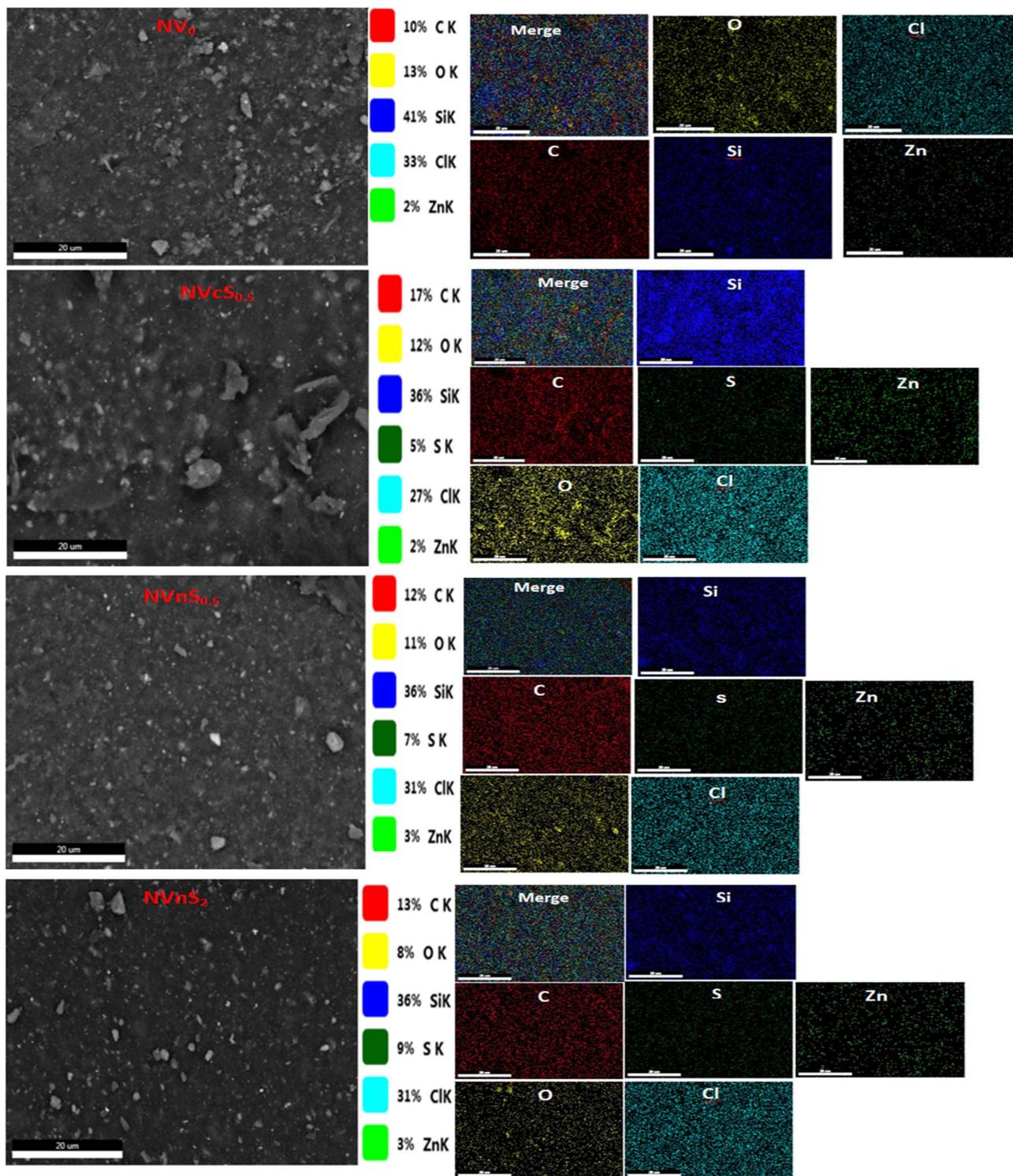
Fig. 9 SEM–EDX elemental mapping images of selected unirradiated NBR/PVC blends, illustrating the distribution and dispersion of different elements in the blend morphology.

unirradiated blends, including the blank (sulfur-free) sample and those containing C-S (0.5 phr) and S-NPs at loadings of 0.5 and 2 phr. ZnO particles incorporated in the blend matrix are responsible for the apparent brilliant spots. Additionally, the blend containing 0.5 and 2 phr of S-NPs exhibits a well-

dispersed morphology, as depicted in the figure, which correlates with enhanced mechanical properties.[55]

On the contrary, the blend loaded with C-S shows aggregation of additives throughout the surface, resulting in a deleterious effect on its mechanical properties. The NBR/PVC blends
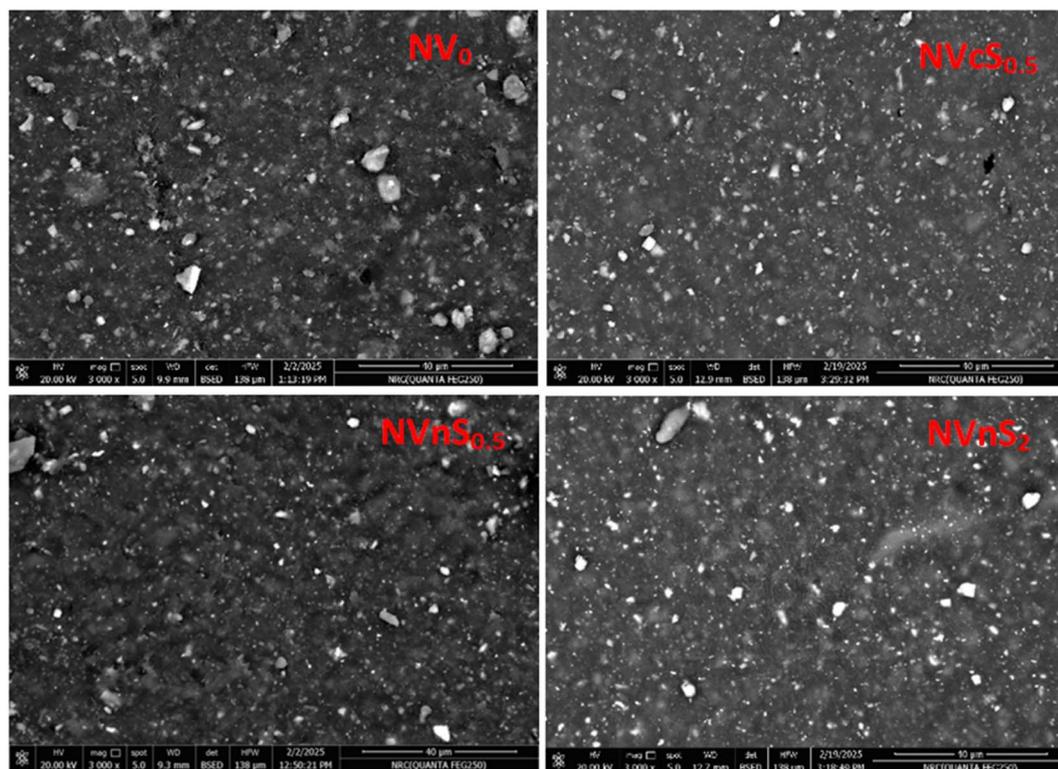
Fig. 10 SEM micrograph of irradiated NBR/PVC blends, showing morphological features and surface characteristics resulting from irradiation.

Table 6 Quantitative agglomerate size analysis of NBR/PVC composites from SEM images (ImageJ)

Sample (SEM image)	Agglomerate count	Total agglomerate area (μm^2)	Average agglomerate size (μm^2)	Agglomerate area fraction (%)
NV_0	194	352.56	1.82	2.61
$NVcS_{0.5}$	249	295.60	1.19	2.11
$NVnS_{0.5}$	92	132.61	1.44	0.94
$NVnS_2$	202	269.04	1.33	1.96

containing S-NPs demonstrated enhanced resistance to crack propagation and improved interfacial adhesion relative to other blends. Fig. 10 illustrates the influence of gamma radiation and S-NP content on the interfacial compatibility of NBR/PVC blends. As shown in Fig. 10, S-NP-filled blends exhibit rougher surfaces after radiation, whereas irradiated blends exhibit brittle, regular fracture surfaces because of radiation-induced crosslinking. The greater restriction of PVC chain mobility caused by crosslinking, which is made possible by the efficient interfacial interaction with the S-NP curing co-agent, is reflected in the radiation-induced alterations in the fracture morphology.[56,57] This enhanced interfacial compatibility is consistent with the improved filler dispersion revealed by quantitative SEM image analysis. A quantitative agglomerate size analysis was conducted using ImageJ to support the qualitative SEM observations. As shown in Table 6, the reference sample NV_0 exhibited the largest average agglomerate size (1.82 μm^2) and area fraction (2.61%). In contrast, samples containing commercial sulfur ($NVcS_{0.5}$) and sulfur nanoparticles ($NVnS_{0.5}$–

$NVnS_2$) showed reduced agglomerate sizes (1.19–1.44 μm^2) and lower area fractions (0.94–2.11%). The lowest area fraction was observed for $NVnS_{0.5}$, indicating a more homogeneous dispersion. These results quantitatively confirm the improved filler dispersion observed in the SEM images.

4. Conclusion

This study demonstrates the successful synthesis of sulfur nano-particles (S-NPs) and their application as a vulcanizing agent in NBR/PVC blends under gamma irradiation. The formation of S-NPs was confirmed via XRD, TEM, and SEM/EDX analyses. The influence of S-NPs on the rheological and physicomechanical properties of unirradiated and irradiated blends was systematically evaluated, along with their thermal aging and automotive oil resistance. The findings indicated that S-NPs effectively promoted crosslinking of NBR/PVC blends, even at a low loading of 0.5 phr. The improvement in physicomechanical performance is attributed to the combined

effects of S-NP content and gamma irradiation dose at 50 kGy, leading to the development of a denser three-dimensional crosslinked network. Also, the S-NP-based vulcanizates demonstrated enhanced resistance to thermal aging and oil exposure under the tested conditions. Thermodynamic analysis revealed improved compatibility and elastic behavior with increasing S-NP content, as indicated by increasing negative ΔG values, reaching a minimum at NVnS$_2$ (2 phr).

Overall, the findings from this work provide a strong foundation for developing advanced, cost-effective NBR/PVC blends with improved performance, setting the stage for future innovations in polymer vulcanization and material design. Overall, the findings from this study provide a strong foundation for developing advanced, cost-effective NBR/PVC blends with improved performance, setting the stage for future innovations in polymer vulcanization and material design.

Author contributions

Doaa S. Mahmoud: conceptualization, data curation, investigation, methodology, visualization, writing – original draft, writing – review & editing. Mohamad Bekhit: conceptualization, data curation, investigation, methodology, visualization, writing – original draft, writing – review & editing. Salwa H. El-Sabbagh: conceptualization, data curation, methodology, supervision, writing – review & editing. E. S. Fathy: conceptualization, data curation, investigation, methodology, writing – review & editing.

Conflicts of interest

The authors declare that there are no conflicts of interests regarding the publication of this paper.

Data availability

Data are available within the article.

References

1 A. G. Chmielewski, M. Haji-Saeid and S. Ahmed, *Nucl. Instrum. Methods Phys. Res., Sect. B*, 2005, **236**, 44–54.
2 Z. Ali, K. El-Nemr, H. Youssef and M. Bekhit, *J. Polym. Compos.*, 2013, **34**, 1600–1610.
3 M. Y. Elnaggar, N. A. Mazied, M. M. Hassan and E. S. Fathy, *J. Vinyl Addit. Technol.*, 2020, **26**, 577–585.
4 M. Y. Elnaggar, E. S. Fathy and R. Okasha, *Polym. Bull.*, 2022, **79**, 9859–9880.
5 M. Bekhit, E. S. Fathy, A. Sharaf and M. Shiple, *Sci. Rep.*, 2024, **14**, 4144.
6 N. Bansal and S. Arora, *Nucl. Instrum. Methods Phys. Res., Sect. B*, 2024, **549**, 165297.
7 A. M. El Sayed, *J. Energy Storage*, 2024, **82**, 110609.
8 M. Kishore, S. A. M. Hussein, F. M. Abdoon, G. N. H. Bindu, A. A. Hamad, K. K. Saxena, R. Gowtham Raj, A. Kumar and T. Srinivas, *Chem. Phys. Impact*, 2025, **11**, 100953.
9 M. M. Dharmaraj, B. C. Chakraborty, B. K. Behera, D. B. Rahim and S. P. J. Sheriff, *J. Polym. Res.*, 2024, **31**, 374.
10 C. Thoral, G. Soulagnet, P.-O. Bussiere and S. Therias, *Polym. Degrad. Stab.*, 2024, **220**, 110633.
11 M. C. S. Perera, U. S. Ishiaku and Z. A. M. Ishak, *Polym. Degrad. Stab.*, 2000, **68**, 393–402.
12 A. V. Maciel, J. C. Machado and V. M. D. Pasa, *Fuel*, 2013, **113**, 679–689.
13 N. Subramanian, K. Senthilvel and B. Prabu, *Mater. Today: Proc.*, 2021, **38**, 2810–2816.
14 M. Hafezi, S. N. Khorsani, F. Ziaei, H. R. Azim and J. Elastomers, *Plastics*, 2007, **39**, 151–163.
15 E. S. Fathy, M. Y. Elnaggar and M. M. Hassan, *Egyptian Journal of Radiation Sciences and Applications*, 2018, **31**, 1–11.
16 S. Atef, D. E. El-Nashar, A. H. Ashour, S. El-Fiki, S. U. El-Kameesy and M. Medhat, *Polym. Bull.*, 2020, **77**, 5423–5438.
17 A. Abbasi, M. M. Nasef and W. Z. N. Yahya, *Green Mater.*, 2020, **8**, 1–8.
18 R. A. Dop, D. R. Neill and T. Hasell, *ACS Appl. Mater. Interfaces*, 2023, **15**, 20822–20832.
19 L. Qin, L. Yang, X. Liu, K. Li, J.-P. Cao and J. Zhang, *Carbon*, 2024, **230**, 119570.
20 R. G. Chaudhuri and S. Paria, *J. Colloid Interface Sci.*, 2010, **343**, 439–446.
21 S. Shankara, R. Pangenib, J. W. Parkb and J.-W. Rhim, *Mater. Sci. Eng., C*, 2018, **92**, 508–517.
22 D. S. Mahmoud, E. M. Eldesouki and W. M. Abd El-Gawad, *Mater. Chem. Phys.*, 2024, **313**, 128673.
23 D. S. Mahmoud, K. S. Abdel Zaher, S. H. El-Sabbagh, A. M. Yossef and G. A. M. Nawwar, *Sci. Rep.*, 2025, **15**, 25363.
24 D. S. Mahmoud, A. M. Soliman, F. M. Helaly and S. H. El-Sabbagh, *BMC Chem.*, 2025, **19**, 315.
25 P. J. Flory and J. Rehner, *J. Chem. Phys.*, 1943, **11**, 521–526.
26 Y. Liu, J. Guo, J. Zhang, Q. Su and G. Du, *Appl. Surf. Sci.*, 2015, **324**, 399–404.
27 R. Mukkabla, P. Meduri, M. Deepa and P. Ghosal, *Chem. Eng. J.*, 2016, **303**, 369–383.
28 A. Beníteza, D. D. Lecceb, Á. Caballeroa, J. Moralesa, E. Rodríguez-Castellónc and J. Hassoun, *J. Power Sources*, 2018, **397**, 102–112.
29 R. M. Tripathi, R. P. Rao and T. Tsuzuki, *RSC Adv.*, 2018, **8**, 36345.
30 Z. Ghoraba, B. Aibaghi and A. Soleymanpour, *J. Chromatogr. B*, 2017, **1063**, 245–252.
31 F. Z. Mohammed, M. Hammadi and M. AL-dulaimi, *Biochemistry Letters*, 2018, **13**, 109–128.
32 A. Swiderska-Mocek, E. Rudnicka and A. Lewandowski, *J. Solid State Electrochem.*, 2020, **24**, 1157–1164.
33 O. M. Bankole, T. D. Olorunsola and A. S. Ogunlaja, *J. Photochem. Photobiol., A*, 2021, **405**, 112934.
34 M. Moghri, A. R. Zanjanijam, L. Seifi and M. Ramezani, *J. Inorg. Organomet. Polym. Mater.*, 2017, **27**, 264–273.
35 T. T. Nghiem, B. L. Nguyen, L. T. Huyen and S. Kawahara, *Polym. J.*, 2023, **55**, 1097–1102.
36 K. Rajkumar, P. Ranjan, P. Thavamani, P. Jeyanthi and P. Pazhanisamy, *J. Chem.*, 2013, **6**, 122.

37 X. Li, Y. Li, C. Qian, S. Wang and R. Nie, *Mater. Today Commun.*, 2024, **39**, 108704.

38 A. A. Abdelsalam, W. S. Mohamed, G. Abd El-Naeem and S. H. El-Sabbagh, *J. Thermoplast. Compos. Mater.*, 2023, **36**, 1811–1832.

39 S. H. El-Sabbagh, A. Nassar, A. A. Ward and D. S. Mahmoud, *Egypt. J. Chem.*, 2024, **67**, 247–256.

40 H. Nabil, H. Ismail and A. R. Azura, *Polym. Test.*, 2013, **32**, 385–393.

41 E. S. Fathy, M. Y. Elnaggar and H. A. Raslan, *J. Vinyl Addit. Technol.*, 2019, **25**, E166–E173.

42 K. F. El-Nemr, M. Y. El-Naggar and E. S. Fathy, *J. Vinyl Addit. Technol.*, 2018, **24**, 37–43.

43 R. O. Aly, M. M. Hassan, J. A. Hasanen and E. F. El Sayed, *J. Appl. Polym. Sci.*, 2012, **124**, 4098–4106.

44 M. Y. Elnaggar, E. S. Fathy and L. A. Wahab, *Appl. Organomet. Chem.*, 2023, **37**, e6965.

45 M. A. Elhady, A. M. Elbarbary, Y. H. Gad and E. S. Fathy, *Polym. Degrad. Stab.*, 2022, **202**, 110012.

46 H. S. Othman, S. H. El-Sabbagh and G. A. Nawwar, *Pigm. Resin Technol.*, 2025, **54/3**, 343–354.

47 A. I. Khalaf, A. A. Yehia, M. N. Ismail and S. H. El-Sabbagh, *Open J. Org. Polym. Mater.*, 2012, **2**, 88–93.

48 M. A. Kader and A. K. Bhowmick, *Polym. Degrad. Stab.*, 2003, **79**, 283–295.

49 M. M. Alam, M. F. Mina and F. Akhtar, *Polym.-Plast. Technol. Eng.*, 2003, **42**, 533–542.

50 S. E. Gwaily, M. M. Badawy, H. H. Hassan and M. Madani, *Polym. Test.*, 2003, **22**, 3–7.

51 H. A. Raslan, E. S. Fathy and S. E. Abdel Aal, *Prog. Rubber, Plast. Recycl. Technol.*, 2023, **39**, 40–63.

52 N. R. Manoj and P. P. De, *Polymer*, 1998, **39**, 733–741.

53 D. Amanda, T. Kemala, J. Rachmadetin, S. G. Sukaryo, A. Cifriadi, M. Khotib, K. Heriyanto and A. Ramadhani, *Urania: Jurnal Ilmiah Daur Bahan Bakar Nuklir*, 2025, **31**, 122–128.

54 A. T. Naikwadi, B. K. Sharma, K. D. Bhatt and P. A. Mahanwar, *Front. Chem.*, 2022, **10**, 837111.

55 R. Luo, D. Kang, C. Huang, T. Yan, P. Li, H. Ren and Z. Zhang, *Polymers*, 2023, **15**, 3723.

56 X. Li, Y. Li, C. Qian, S. Wang and R. Nie, *Mater. Today Commun.*, 2024, **39**, 108704.

57 N. K. Gupta, S. Gupta and A. Tedesse, *J. Polym. Res.*, 2022, **9**, 119.